Long-range guided THz radiation by thin layers of water

Robert Sczech,[1] **Jaime Gómez Rivas,**[2,3,*] **Audrey Berrier,**[2] **Vincenzo Giannini,**[2] **Giuseppe Pirruccio,**[2] **Christian Debus,**[1] **Heiko Schäfer-Eberwein,**[1] **and Peter Haring Bolívar**[1]

[1] *Institute of High Frequency and Quantum Electronics (HQE), University of Siegen, Hölderlinstrasse 3, 57076 Siegen, Germany*

[2] *Center for Nanophotonics, FOM Institute AMOLF, c/o Philips Research Laboratories, High Tech Campus 4, 5656 AE Eindhoven, The Netherlands*

[3] *COBRA Research Institute, Eindhoven University of Technology, P.O. Box 513, 5600 MB Eindhoven, The Netherlands*

[*]*rivas@amolf.nl*

Abstract: We propose a novel method to guide THz radiation with low losses along thin layers of water. This approach is based on the coupling of evanescent surface fields at the opposite sides of the thin water layer surrounded by a dielectric material, which leads to a maximum field amplitude at the interfaces and a reduction of the energy density inside the water film. In spite of the strong absorption of water in this frequency range, calculations show that the field distribution can lead to propagation lengths of several centimeters. By means of attenuated total reflection measurements we demonstrate the coupling of incident THz radiation to the long-range surface guided modes across a layer of water with a thickness of 24 μm. This first demonstration paves the way for THz sensing in aqueous environments.

OCIS codes: (230.7390) Waveguides, planar; (050.6624) Subwavelength structures; (310.2790) Guided waves; (040.2235) Far infrared or terahertz; (300.6495) Spectroscopy, terahertz.

References and links

1. K.H. Yang, P.L. Richards, and Y.R. Shen, "Generation of far-infrared radiation by picosecond light pulses in LiNbO$_3$," Appl. Phys. Lett. **19**, 320-323 (1971).
2. D.H. Auston, A.M. Glass, and A.A. Ballman, "Optical rectification by impurities in polar crystals," Phys. Rev. Lett. **28,** 897-900 (1972).
3. S.L. Dexheimer, *Terahertz Spectroscopy: Principles and Applications (ed.)* (CRC Press, 2008).
4. B. Ferguson, and X. Zhang, "Materials for terahertz science and technology," Nat. Materials **1**, 26-33 (2002).
5. B. M. Fischer, M. Walther, and P.U. Jepsen, "Far-infrared vibrational modes of DNA components studied by terahertz time-domain spectroscopy," Phys. Med. Biol. **47**, 3807-3814 (2002).
6. O. P. Cherkasova, M. M. Nazarov, A. P. Shkurinov, and V. I. Fedorov, "Terahertz spectroscopy of biological molecules," Radiophys. and Quantum Electronics **52**, 518-523 (2009).
7. X-C Zhang, "Terahertz wave imaging: horizons and hurdles," Phys. Med. Biol. **47** 3667-3677 (2002).
8. J.A. Zeitler, P.F. Taday, D.A. Newnham, M. Pepper, K.C. Gordon, and T. Rades, "Terahertz pulsed spectroscopy and imaging in the pharmaceutical setting - a review," J. Pharm. Pharmacol. **59**, 209-223 (2007).
9. G. Gallot, S.P. Jamison, R.W. McGowan, and D. Grischkowsky, "Terahertz waveguides," J. Opt. Soc. Am. B **17**, 851-863 (2000).
10. K. Wang, and D.M. Mittleman, "Metal wires for terahertz wave-guiding," Nature **432**, 376-379 (2004).
11. J. Zhang, and D. Grischkowsky, "Waveguide terahertz time-domain spectroscopy of nanometer water layers," Opt. Lett. **29**, 1617-1619 (2004).

12. J. Liu, R. Mendis, and D.M. Mittleman, "The transition from a TEM-like mode to a plasmonic mode in parallel-plate waveguides," Appl. Phys. Lett. **98**, 231113 (2011).
13. B.K. Juluri, Sz.-C.S. Lin, T.R. Walker, L. Jensen, and T.J. Huang, "Propagation of designer surface plasmons in structured conductor surfaces with parabolic gradient index," Opt. Express **17**, 2997-3006 (2009).
14. A.I. Fernández-Domínguez, E. Moreno, L. Martín-Moreno, and F.J. García-Vidal, "Guiding terahertz waves along subwavelength channels," Phys. Rev. B **79**, 233104 (2009).
15. N. Yu, Q.J. Wang, M.A. Kats, J.A. Fan, S.P. Khanna, L.Li, A.G. Davies, E.H. Linfield, and F. Capasso, "Designer spoof-surface-plasmon structures collimate terahertz laser beams," Nature Mater. **9**, 730-735 (2010).
16. D. Martin-Cano, M.L. Nesterov, A.I. Fernández-Domínguez, F.J. García-Vidal, L. Martín-Moreno, and E. Moreno, "Domino plasmons for subwavelength terahertz circuitry," Opt. Express **18**, 754-764 (2010).
17. A.W. Snyder, and J.D. Love, *Optical waveguide theory* (Chapman and Hall, 1983).
18. R. Mendis, and D. Grischkowsky, "Plastic ribbon THz waveguides," J. Appl. Phys. **88**, 4449-4451 (2000).
19. P. Yeh, *Optical waves in layered media* (John Wiley and Sons, 1988).
20. H. Raether, *Surface Polaritons on Smooth and Rough Surfaces and on Gratings* (Springer-Verlag, 1988).
21. D. Sarid, "Long-range surface-plasma waves on very thin metal films," Phys. Rev. Lett. **47**, 1927-1930 (1981).
22. P. Berini, "Long range surface plasmon polaritons," Adv. Opt. Photon. **1**, 484-588 (2009).
23. Y. Zhang, A. Berrier, and J. Gómez Rivas, "Long range surface plasmon polaritons at terahertz frequencies in thin semiconductor layer," Chin. Opt. Lett. **9**, 110014 (2011).
24. L.H. Smith, M. C. Taylor, I. R. Hooper, and W.L. Barnes, "Field profiles of coupled surface plasmon-polaritons," J. Mod. Opt. **55**, 2929-2943 (2008).
25. G. J. Kovacs, "Surface polariton in the ATR angular spectra of a thin iron film bounded by dielectric layers," J. Opt. Soc. Am. **68**, 1325-1332 (1978).
26. F. Yang, J. R. Sambles, and G. W. Bradberry, "Long-Range surface modes supported by thin films," Phys. Rev. B **44**, 5855-5872 (1991).
27. V. Giannini,Y. Zhang, M. Forcales, and J. Gómez Rivas, "Long-range surface polaritons in ultra-thin films of silicon," Opt. Express **16**, 19674 (2008).
28. C. Arnold, Y. Zhang, and J. Gómez Rivas, "Long range surface polaritons supported by lossy thin films," Appl. Phys. Lett. **96**, 113108 (2010).
29. Y. Zhang, C. Arnold, P. Offermans, and J. Gómez Rivas, "Surface wave sensors based on nanometric layers of strongly absorbing materials," Opt. Express **20**, 9431-9441 (2012).
30. H.J. Liebe, G.A. Hufford, and T. Manabe, "A model for the complex permittivity of water at frequencies below 1 THz," Int. J. Infrared Milli. **12**, 677682 (1991).

1. Introduction

The development of terahertz (THz) technology is consolidating new applications in this frequency range of the electromagnetic spectrum [1–3]. In particular, electromagnetic radiation at THz frequencies has a large potential for sensing given the resonant response of many elementary low-energy excitations in this frequency range [3,4]. THz radiation has been proven to be a valuable tool for the spectroscopy of DNA, aminoacids and proteins [5,6]. However, one of the largest hurdles of THz for biomolecular analysis is the strong optical absorption of water and buffer solutions in which biomolecules are preserved [7]. Up to now, this strong absorption has hampered THz spectroscopy in aqueous solutions. Therefore, defining new concepts to overcome water absorption in THz applications will lead to an ample range of possibilities for spectroscopy and sensing in this frequency range [8].

In this manuscript we demonstrate a novel concept to guide THz radiation with low losses along water films. Over the past few years intensive research has been carried out on the definition of novel waveguides to confine and guide THz radiation over long distances. This research has led to photonic and plasmonic waveguides [9–12] and waveguides based on subwavelength structures [13–16]. A common denominator in all these guiding structures is that material absorption is minimized in order to achieve long propagation lengths. Here, we demonstrate that it is possible to excite the long-range guided mode, in spite of the strong absorption of water at THz frequencies. In contrast to the well-known concept of TM_0 modes in low absorbing dielectric slab waveguides, the investigated slab waveguide structure in this work deviates from this standard situation [17] as the core layer material is a highly absorbing material and the waveguide has to remain significantly thinner in order to allow low-loss propagation [18]. The

coupling of the electromagnetic field at the opposite sides of the layer leads to an evanescent surface mode that propagates over long distances. This mode corresponds to the fundamental TM$_0$ mode guided in a waveguide formed by a strongly absorbing material and surrounded by a non-absorbing dielectric. The symmetry of the electromagnetic field, which leads to a reduction of the energy density inside the water layer, is responsible for the long propagation of the guided mode in the thin film.

The manuscript is organized as follows. In section 2 we discuss the dispersion of the eigenmodes in absorbing slabs and demonstrate that it is possible to achieve the condition for long-range waveguiding along water films. The fabrication of the water layers is described in section 3. In section 4 we present the experimental demonstration of the excitation of long-range guided modes in water layers at THz frequencies. This demonstration is realized by measuring the total internal reflection at the interface between a coupling prism and the sample when the matching conditions to the guided mode are met. We note that although this configuration does not allow a direct measurement of the propagation length, it confirms the coupling of incident THz radiation to evanescent guided modes in excellent agreement with calculations. The manuscript is ended with the conclusions in section 5.

2. Guided modes along absorbing thin layers

The dispersion relation describing the eigenmodes supported by a slab of a medium with a complex permittivity $\varepsilon_2 = \varepsilon_{r,2} + i\varepsilon_{i,2}$ and thickness d, surrounded by two lossless dielectrics characterized by the permittivities ε_1 and ε_3, can be derived by applying the electromagnetic boundary conditions to the field components at the two interfaces [19, 20]. For the case of TM polarized modes, this leads to the following expression

$$e^{-2i\beta_{z2}d} = \left(\frac{\frac{\beta_{z2}}{\varepsilon_2} + \frac{\beta_{z1}}{\varepsilon_1}}{\frac{\beta_{z2}}{\varepsilon_2} - \frac{\beta_{z1}}{\varepsilon_1}} \right) \left(\frac{\frac{\beta_{z2}}{\varepsilon_2} + \frac{\beta_{z3}}{\varepsilon_3}}{\frac{\beta_{z2}}{\varepsilon_2} - \frac{\beta_{z3}}{\varepsilon_3}} \right) , \tag{1}$$

where β_{zj} is the wave vector component normal to the slab in medium j. This wave vector component is related to the propagation constant of the guided modes in the slab, β_x, by $\beta_x^2 + \beta_{zj}^2 = \varepsilon_j k_0^2$, where k_0 is the wave number in vacuum.

If we assume that the slab is symmetrically surrounded by the same dielectric, i.e., $\varepsilon_1 = \varepsilon_3$ and $\beta_{z1} = \beta_{z3}$, Eq. (1) has two solutions

$$\tanh\left(i\beta_{z2}d/2\right) = -\frac{\varepsilon_2\beta_{z1}}{\varepsilon_1\beta_{z2}} , \tag{2}$$

and

$$\tanh\left(i\beta_{z2}d/2\right) = -\frac{\varepsilon_1\beta_{z2}}{\varepsilon_2\beta_{z1}} . \tag{3}$$

These two equations correspond to symmetric and antisymmetric TM eigenmodes in slab waveguides, where the symmetry refers to the magnetic field component H$_y$ with respect to the middle plane of the slab. The symmetric and antisymmetric modes have been intensively investigated in thin metallic slabs at optical frequencies [21, 22]. They have been also proposed in semiconductor slabs at THz frequencies [23]. Common in these studies is that the real component of the permittivity of the material forming the slab in the frequency range of interest is negative. This represents the condition of a conductor that supports surface plasmon polaritons (SPPs), i.e., surface waves at the interfaces decaying evanescently into the dielectric and the conductor. The SPPs at the opposite side of the slab can couple with each other when their penetration depth is larger than the thickness of the slab. This coupling is only effective if the

momentum (or in-plane wave number along the slab) of both SPPs is similar, which is achieved only if the refractive indices of the dielectrics surrounding the slab are comparable. As a result of the coupling, the SPPs at the opposite side hybridize, forming the symmetric or long-range SPPs (Eq.(2)) and antisymmetric or short-range SPPs (Eq.(3)). The terms long-range and short-range surface modes arise from the respective long and short propagation lengths of these modes compared to the propagation of SPPs on single interfaces. These propagation lengths are the result of the reduced or increased absorption due to the field distribution in the conducting layer [24].

In 1978 Kovacs demonstrated that high losses in thin slabs of metals is not an impediment for the excitation of long-surface surface modes [25]. This work was extended by Yang and co-workers to non-metallic materials with very large absorption at infrared frequencies [26]. Giannini *et al.* [27] and Arnold *et al.* [28] demonstrated the excitation of long-range guided modes at optical frequencies in strongly absorbing films. These modes, described by Eq. (2), result from the coupling of the evanescent fields at opposite side of the absorbing film. Recently, they have been proposed for optical sensing at short wavelengths [29]. Accordingly, Eq. (3) defines also the dispersion of short-range modes in thin layers of absorbing dielectrics. However, these short-range modes are leaky waves that do not propagate along the slab [26, 27].
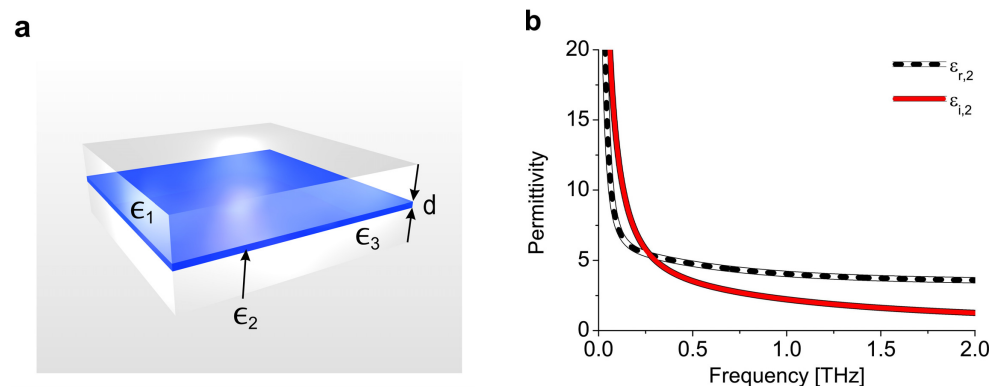
a

b

Fig. 1: (a) Schematic (not to scale) of a triple layer system consisting of an absorbing layer with thickness d homogeneously surrounded by low loss dielectrics with the permittivities ε_1 and ε_3. (b) Real and imaginary components of the permittivity of water at 21 °C.

In order to illustrate the characteristic lengths of long-range guided modes along water films, we consider the system formed by a thin layer of water homogeneously surrounded by a lossless and non-dispersive dielectric with permittivity $\varepsilon_1 = \varepsilon_3 = 2.36$. A graphical representation of such a triple layer structure is shown in Fig. 1(a). The permittivity of water is calculated using a double Debye relaxation model reported in literature [30]. Figure 1(b) displays the real and imaginary components of the permittivity of bulk water at room temperature as a function of the frequency. The permittivity is characterized by a positive real component and a large imaginary component with an increasing value for decreasing frequencies. At frequencies lower than 0.3 THz, the imaginary component of the permittivity is even larger than the real component.

Figure 2(a) displays the calculated intensity propagation lengths L_x as a function of the frequency of long-range guided modes for different water layer thicknesses. These values are calculated by solving Eq. 2 to obtain the complex propagation constant β_x [26]. The propagation length is defined as $1/(2|\Im(\beta_x)|)$, where $\Im(\beta_x)$ is the imaginary component of β_x. Long-range guided modes show an enhanced propagation length for thin layers that can be up to four orders

of magnitude larger than that of THz radiation in bulk water at room temperature for sufficiently thin layers and at low frequencies. The origin for this long propagation length can be found in the distribution of the electromagnetic field around the thin layer. This is illustrated in Fig. 2(b), where the propagation length L_x along the thin layer and the decay length L_z of the electromagnetic field from the thin layer into the surrounding media are represented as a function of the thickness of that layer. The calculations are performed for 0.48 THz and the propagation and decay lengths are given in units of the corresponding wavelength, i.e., 625 μm. The intensity decay length L_z is calculated from $1/(2|\Im(\beta_{zj})|)$ with j = 1,3. As it is emphasized with Fig. 2(b), the increase in the propagation length is associated with an increase of the decay length into the surrounding dielectric. Due to the coupling of the fields on the opposite side of the water layer, the field is repelled from this layer, minimizing the absorption. The shaded area in Fig. 2(b) marks the range of thicknesses of the water layer at which the field is well confined, i.e., $L_z < \lambda$, while the guided mode still propagates along that layer, i.e., $L_x > \lambda$.
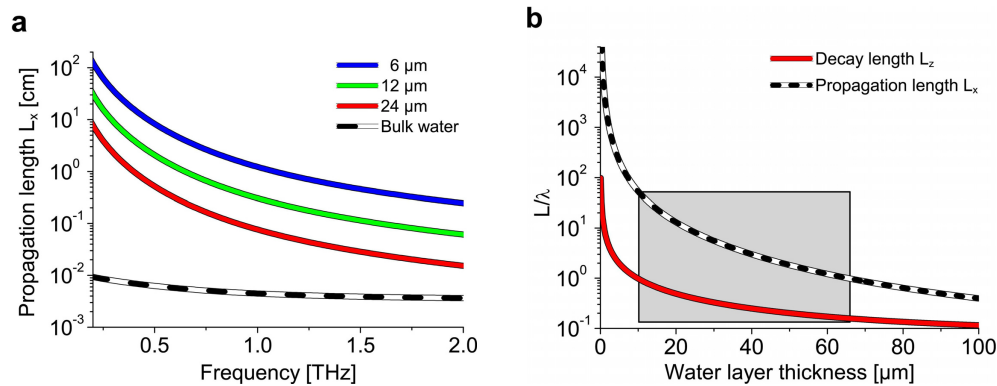

Fig. 2: (a) Calculated intensity propagation lengths as a function of frequency of long-range guided modes along layers of water (T = 21°C) with a thickness d = 6 μm, 12 μm and 24 μm, surrounded by a lossless dielectric with a permittivity of 2.36. The dashed line represents the absorption length of THz radiation in water. (b) Intensity propagation length and decay length into the surrounding dielectric of long-range guided modes, normalized to the wavelength λ = 625 μm, as a function of the thickness of the water layer for a lossy dielectric with $\varepsilon_2 = 4.8 + 3.6i$.

3. Sample fabrication

The water layer was fabricated in the clean room using standard lithographic techniques. We have fabricated several 3 mm TOPAS (Topas Advanced Polymers, inc.) / water layer / 250 μm Zeonor (Zeon Corporation) triple layer samples. The choice of different polymers for the lower and upper medium surrounding the water film is determined by the manufacturing process. Nevertheless, TOPAS and Zeonor have very similar refractive indices, $\varepsilon_{\text{Zeonor}} \approx 2.3596 + 0.0154i$ and $\varepsilon_{\text{TOPAS}} \approx 2.3611 + 0.0015i$, practically preserving the uniformity of the media surrounding the water layer. In order to give rigidity to the water film, avoiding the bending and collapse of the upper Zeonor layer onto the substrate, micropillars with a diameter of 20 μm and the height of the water layer were randomly arranged onto the substrate during the micromaching process. The diameter of these micropillars is much smaller than the wavelength of THz radiation and their density was kept low to avoid any disturbance in the coupling of the incident THz radiation to the long-range guided mode. The overall area occupied by the 24 pillars within the compartment is less than 10^{-4}%. Their random distribution was chosen in order to avoid any standing waves induced by a regular micropillar arrangement. This fabrication was done by UV lithography of the spin coated negative photo resist SU 8 (Micro Resist Technology GmbH). The 2.4 x 4 cm^2 water compartment and micro fluidic chan-

nels with a width of 500 μm, used to fill the water layer, were fabricated with the same process. Several samples were fabricated with water films having a thickness ranging from 17 μm to 24 μm. The micro patterned substrate and top Zeonor layer were fused together by a thermal bonding process under moderate pressure at 100 °C for 24 h giving rise to triple layer structures as that shown in Fig. 3(a).
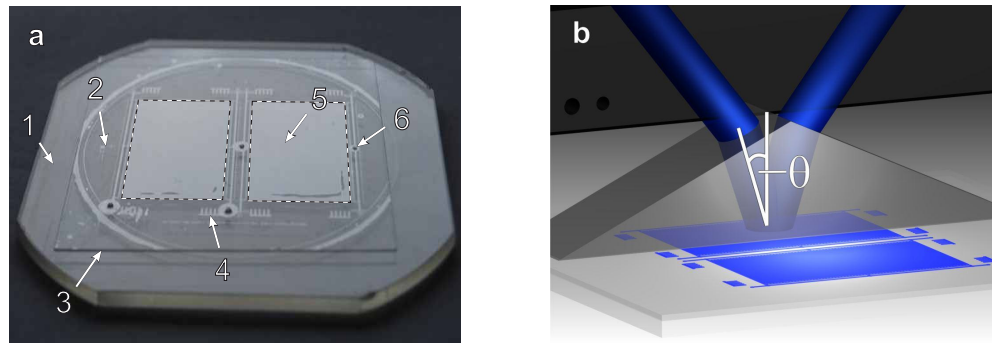

Fig. 3: (a) Photograph of the triple layer structure consisting of 3 mm thick TOPAS substrate (1), 250 μm Zeonor cover slide (2), SU-8 photoresist (3), micropatterned markers for prism positioning (4), 2.4 x 4 cm^2 water compartments indicated by the black dotted boundaries (5) and water filling hole (6). (b) Schematic representation of the setup used to couple free-space THz radiation to long-range guided modes in thin layers of water.

4. Attenuated total reflection measurements

A commonly used technique to couple free space radiation to evanescent modes is the attenuated total reflection (ATR), schematically represented in Fig. 3(b). A high refractive index prism is brought in contact with the upper layer of the sample, i.e., the Zeonor layer. We use a silicon prism in our experiments. The prism is illuminated by a plane wave at an angle larger than the critical angle of total internal reflection at the prism-Zeonor interface. For these angles the wave is evanescently transmitted into the Zeonor with an in-plane wave number equal to that in the prism. This evanescently transmitted field can couple to surface guided modes in the triple layer sample. A strong reduction of the specular reflection is then observed indicating the coupling of the incident wave to the eigenmode guided by the thin water film. Figures 4(a) - 4(c) show the calculations of the field components for the excited long-range guided mode in the multilayer structure normalized to the incident field. These calculations are performed by solving Maxwell equations and applying the electromagnetic boundary conditions. All 3 components of the electromagnetic field are calculated for a p-polarized plane wave incident at the angle θ_c under resonant coupling conditions to the surface guided mode. The upper medium represents the Si prism (I) and the vertical scale of the water film is magnified in order to highlight the field component distribution inside this layer. The electric field component E_x along the propagation direction (Fig. 4(a)) couples antisymmetrically across the water layer, whereas E_z (Fig. 4(b)) is symmetrically distributed with respect to the middle plane of the high absorbing water layer. While both field components have their maxima near the interfaces, decaying exponentially into the surrounding dielectrics, the magnetic field component H_y (Fig. 4(c)) shows its maximum value inside the water layer. Hence, the energy density associated to the electric field and the dielectric absorption are reduced inside the water layer, leading to the long propagation length of these modes. We note that despite of the significant energy density reduction inside the water layer, a fraction of the electric field remains inside the thin water layer. This characteristic makes long-range guided modes useful for THz sensing in aqueous environments.
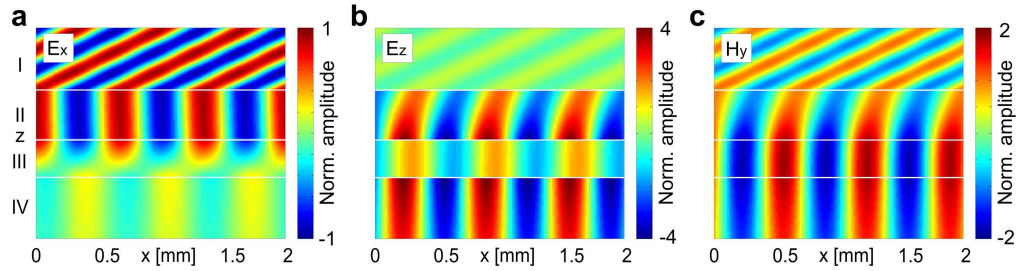
Fig. 4: Calculation of the field amplitudes, normalized by the incident fields, in the prism (I) and the triple layer (Zeonor top layer (II), water layer (III) and TOPAS substrate (IV)). A p-polarized plane wave with a vacuum wavelength of 625 μm is incident from the prism exciting a long-range mode guided in the water layer. (a) The electric field component of this mode along the propagation direction, E_x, (b) E_z field component along the direction normal to the water layer, and (c) is the magnetic field component H_y. The guiding structure consists of a triple layer formed by a 250 μm thick Zeonor cover slide with $\varepsilon_{\text{Zeonor}} = 2.36 + 0.0154i$, a 24 μm thick water layer with $\varepsilon_{\text{water}} = 4.8 + 3.6i$, and a semi-infinite TOPAS substrate slab with $\varepsilon_{\text{TOPAS}} = 2.36 + 0.0015i$.

In order to excite the long-range mode, the angle of incidence is varied in an ATR experiment and the specular reflection is measured. This technique is integrated with a standard THz time domain spectrometer (THz-TDS) as schematically represented in Fig. 5.
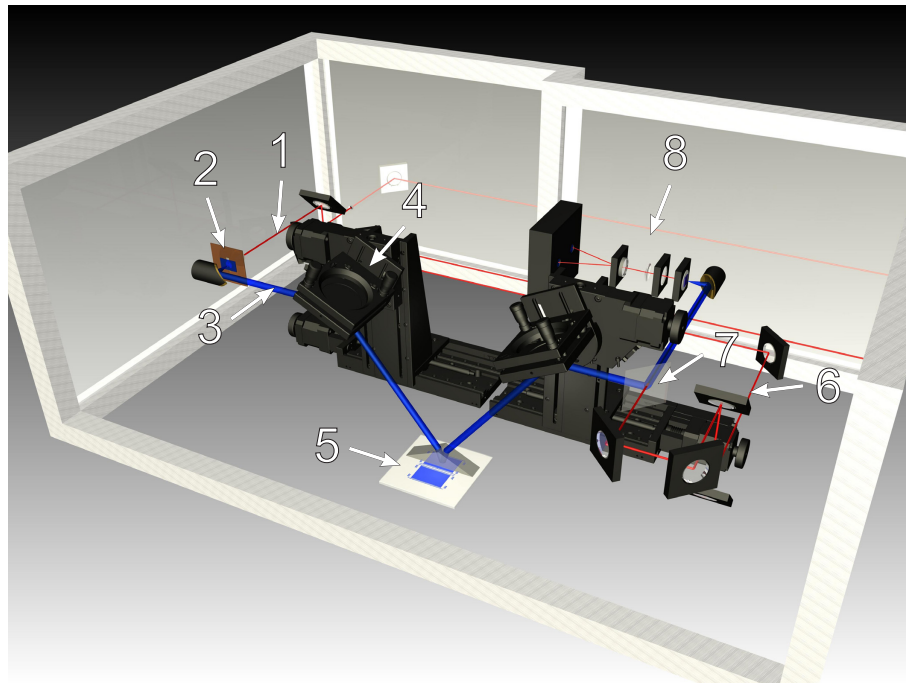

Fig. 5: The THz-TDS attenuated total reflection setup with pump beam for THz generation (1), THz emitter (Au electrodes on GaAs) (2), collimated THz beam (3), Au mirror fixed to rotary stage which is mounted on linear stage (4), prism placed on top of the water containing triple layer structure (5), probe beam for THz detection (6), wavelength dependent reflecting Indium Tin Oxide (ITO) (7) and electrooptic detection unit (8).

The setup enables to measure the field amplitude of THz pulses as a function of the time with sub-ps accuracy. All experiments are carried out under N_2 purged atmosphere. Our setup uses a

large aperture GaAs emitter and an electrooptic detection unit with a ZnTe crystal. A collimated gaussian THz beam is used to enable the angle dependent coupling to the guided mode. In order to scan a complete range of angles, the collimated THz beam is guided to the prism with a planar Au mirror which is mounted on a motorized rotary-/linear stage setup. The angle resolution for scanning is chosen between $0.01°$ and $0.1°$ and the scanning range from $23.5°$ to $28.5°$. Each THz transient in time domain at each discrete angle is recorded and automatically fast Fourier transformed to obtain the reflection spectra. Finally, the reflectivity is obtained by normalizing the reflection at each angle to that measured at $28.5°$. This angle is well beyond the critical angle for total internal reflection ($\theta_c = 26.7°$) and the specular reflection is close to 100% as shown in Figs. 6(a) - 6(c).
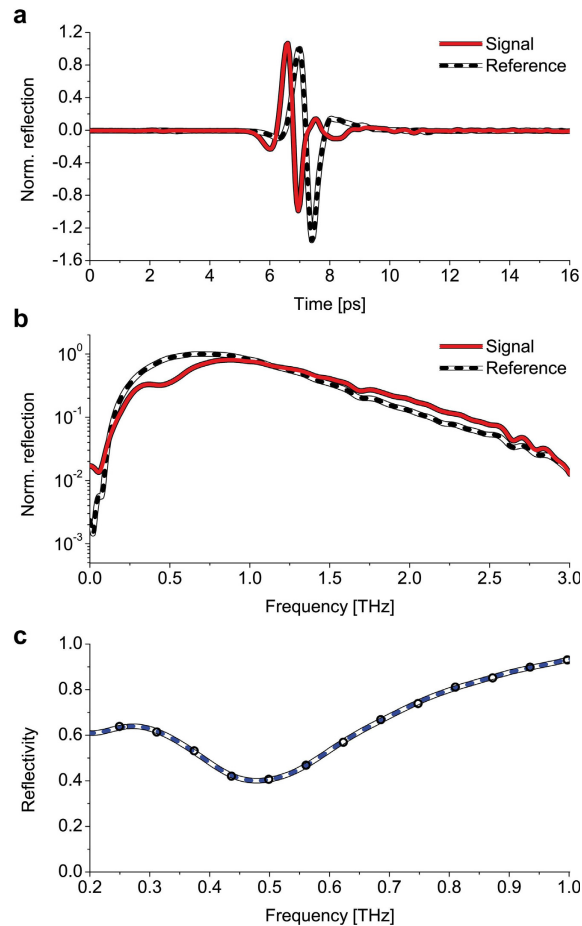

Fig. 6: Representative specular reflection measurement at an angle of $26.8°$ and reference measurement at $28.5°$. (a) Transients, (b) FFT spectra of the transients, (a) and (b) are normalized to the maximum reflection of the reference. (c) Reflectivity calculated from (b). The black circles are the reflectivity data points from the FFT of the non-offset corrected and non-zero padded transients in (a) representing the frequency interval corresponding to the duration in time domain.

Referencing to a gold mirror gives rise to analogous results. However, repositioning inaccuracies when exchanging the sample with the reference mirror lead to larger errors. Figure 6(a) displays an exemplary THz transient measured at $\theta = 26.8°$ (solid curve) and the reference measured at $\theta = 28.5°$ (dashed curve). The amplitude spectra, obtained by fast Fourier trans-

forming, are shown in Fig. 6(b). The main feature in the spectra is the dip observed in the specular reflection for $\theta = 26.8°$ at 0.5 THz. This dip can be better appreciated in the reflectivity spectrum displayed in Fig. 6(c), where the reflectivity is defined as the amplitude spectrum normalized by the spectrum of the reference. The dip corresponds to the resonant coupling of the incident THz radiation to the long-range guided mode along the thin water layer.

The specular reflection measurements as a function of the incidence angle are shown in Figs. 7 - 9. In all experiments an index matching oil (CARGILLE LABS) between prism and sample is used to ensure optical contact to the sample.
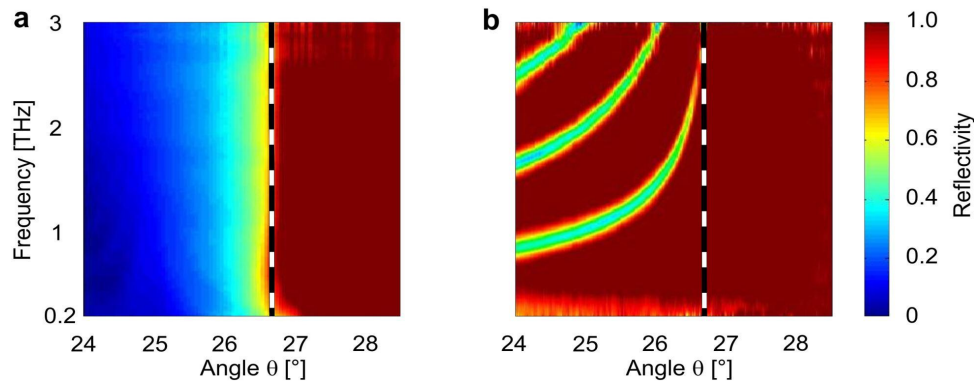

Fig. 7: Attenuated total reflectivity of incident THz radiation in the case of (a) p-polarized waves incident on a 3 mm homogeneous single TOPAS slab / Si prism interface (angle resolution $\theta_r = 0.05°$) and (b) s-polarized waves at a quasi-homogeneous triple layer structure consisting of 250 μm Zeonor cover slide / 24 μm liquid layer / 3 mm TOPAS substrate slab (filled with water) ($\theta_r = 0.03°$). The critical angle (black dashed) line is slightly tilted due to the dispersion of the dielectric materials.

Figure 7(a) shows a control measurement done for a p-polarized incident wave on a homogeneous dielectric sample consisting of a single TOPAS slab with the prism placed on top of it. The measured value of the critical angle of total internal reflection, $\theta_c = 26.7°$, is in excellent agreement with the calculated value (dashed line). As it can be appreciated from Fig. 7(b), s-polarized waves do not couple to the long-range guided mode. However, for angles lower than the critical angle, there are bands with a decreased reflectivity. These bands correspond to Fabry-Perot resonances in the Zeonor layer which has the characteristics of a classical dielectric waveguide. The situation drastically changes when experiments for p-polarization are performed (see Fig. 8). The most remarkable feature is the reduced specular reflectivity at $\theta = 27°$ and 0.5 THz as marked in Fig. 8 with an arrow. This attenuated reflectivity corresponds to the coupling of the incident radiation to the long-range guided mode in the water containing triple layer. Figure 8(b) shows a transfer matrix calculation of the specular reflectivity using the permittivity values for water indicated in Fig. 1(b). The calculation reproduces remarkably well all the features of the measurements and especially the attenuated total reflection around 0.5 THz due to the excitation of the long-range water guided mode. The resonant coupling to long-range guided modes takes place only at defined angles of incidence and frequencies which are determined by the momentum matching conditions. These matching conditions depend on the permittivities of the prism and the three layers forming the sample, as well as on the thickness of the top (Zeonor) layer and the water layer. Therefore, one should expect a change in the reflectivity if the permittivity of the guiding layer is changed. This change is illustrated with the measurements in Fig. 9(a) and confirmed with the calculations shown in Fig. 9(b), where the specular reflection of the sample as before is displayed, but in which the water is replaced by pure ethanol.
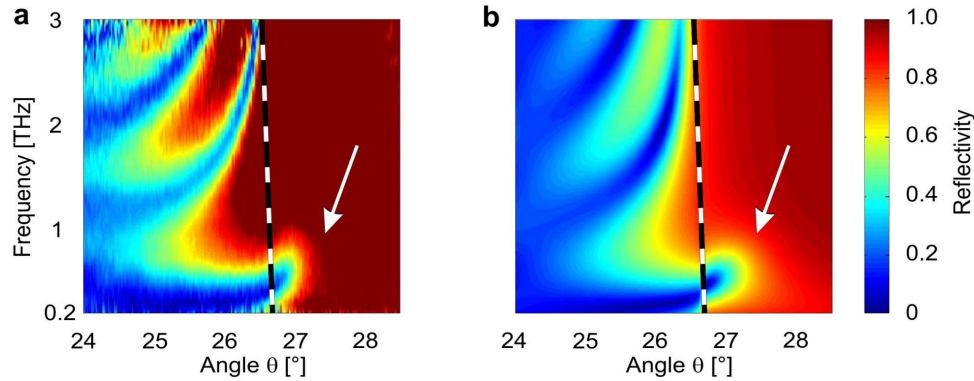
Fig. 8: Attenuated total reflectivity of p-polarized incident THz radiation and coupling to a long-range guided mode (indicated by a white arrow) in a triple layer structure consisting of 250 μm Zeonor cover slide / 24 μm water layer / 3 mm TOPAS substrate slab, (a) experimental data with angle resolution $\theta_r = 0.03°$ and (b) calculation of the specular reflectivity.

The main difference compared to the results of Figs. 8(a) and 8(b) is the strong suppression of the attenuated total reflectivity dip, which is observed for water due to the excitation of the long-range guided mode. We note that the dip is not completely suppressed, which might be due to the coupling of the incident radiation to the TM_0 mode guided by the weakly absorbing ethanol layer. This result indicates that the observed feature at angles above the critical angle is strongly dependent on the permittivity of the liquid layer. It is interesting to note that the Fabry-Perot resonances remain nearly unchanged when the water is replaced by ethanol. This is an expected result as these resonances are caused by the reflection in the Zeonor layer.
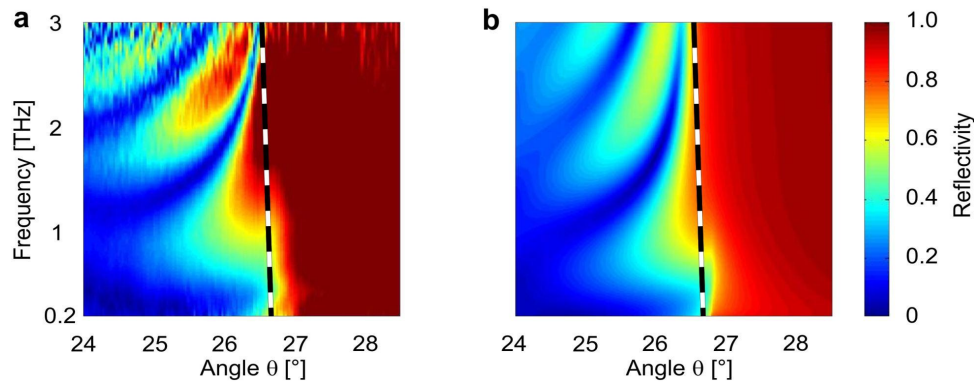

Fig. 9: Attenuated total reflectivity of p-polarized THz radiation incident on a triple layer structure with an ethanol thin layer. The structure consists of 250 μm Zeonor cover slide / 24 μm ethanol / 3 mm TOPAS substrate slab, (a) experimental data with angle resolution $\theta_r = 0.03°$ and (b) transfer matrix calculation of the specular reflectivity.

5.   Conclusions

We have demonstrated the possibility to couple THz radiation into long-range guided modes propagating along highly absorbing water films with attenuated total reflection THz time-domain spectroscopy. The specular reflection for angles larger than the critical angle of total internal reflection at 0.5 THz indicates the long-range guided mode excitation, which is confirmed with transfer matrix calculations. Moreover, our experimental results show that this

feature can be suppressed by changing the dieletric constant of the absorbing layer, i.e., by replacing the highly absorbing water by low absorbing ethanol. Long-range guided modes in thin water films have in theory propagation lengths in the order of centimeters. In contrast to previously reported water-based THz sensing concepts demanding a minimum impact of water absorption for molecular characterization, here the absorption coefficient of water is not a limiting factor. Hence, we anticipate our work to be a starting point for a further research regarding THz detection and spectroscopy of molecules or cells in their native aqueous environment in fields such as clinical diagnostics as well as environmental analysis.

Acknowledgments